Roughness of two nonintersecting one-dimensional interfaces

Janne Juntunen,* Otto Pulkkinen,† and Juha Merikoski‡
Department of Physics, University of Jyväskylä, P.O. Box 35, FI-40014 Jyväskylä, Finland
(Received 31 August 2006; revised manuscript received 3 August 2007; published 25 October 2007)

The dynamics of two spatially discrete one-dimensional single-step model interfaces with a noncrossing constraint is studied in both nonsymmetric propagating and symmetric relaxing cases. We consider possible scaling scenarios and study a few special cases by using continuous-time Monte Carlo simulations. The roughness of the interfaces is observed to be nonmonotonic as a function of time, and in the stationary state it is nonmonotonic also as a function of the strength of the effective force driving the interfaces against each other. This is related on the one hand to the reduction of the available configuration space and on the other hand to the ability of the interfaces to conform to each other.

DOI: 10.1103/PhysRevE.76.041607 PACS number(s): 81.10.Aj, 02.50.Ey, 05.40.−a, 64.60.Ht

I. INTRODUCTION

Discrete stochastic lattice models have been studied extensively in statistical physics to gain insight into the dynamics of physical interfaces between different phases. Usually those models are much easier to solve numerically or analytically than the related stochastic partial differential equations that describe the physics at hydrodynamic scales [1,2]. Often this description is valid already at relatively small length scales corresponding to just a few lattice units, while sometimes long crossover scales are involved.

In Ref. [3], Barabasi introduced a model of two interfaces, where the direction of the local change of one interface was in part determined by the shape of the other, but not affected by their distance. The steady states of general systems of interfaces coupled via differential operators in their effective equations of motion have been studied in Ref. [4]. Also randomly coupled interfaces have been considered [5]. In these models, the interfaces are allowed to intersect.

In adsorption systems more than two phases can coexist and different types of nonintersecting domain walls interact with each other [6–8]. In paper combustion [9,10] smoldering, burning, and fading fronts always are in a specified order. Balankin *et al.* [11] recently presented experimental results for the wetting of paper and described the process as the dynamics of two coupled interfaces: the precursor and main fronts. Models where two or more interfaces cannot cross each other could also describe the internal structure of a phase boundary.

There has also been considerable theoretical interest in noncrossing line ensembles [12] and the related problem of a single Kardar-Parisi-Zhang (KPZ) type interface in the presence of a constraining wall [13–15]. Theoretically, stationary properties of nonintersecting one-dimensional interfaces, such as adjacent steps on a vicinal surface, can also be examined via a mapping onto a one-dimensional fermion or boson system [16].

In Sec. II of this paper we propose a model consisting of two nonintersecting discrete interfaces obeying the body-centered solid-on-solid (BCSOS) restriction. The parameters of the two processes are chosen in such way that the interfaces will interact with each other. We shall consider interfaces propagating as a pair and interfaces driven symmetrically toward each other. After outlining the scaling behavior of the combined system phenomenologically in Sec. III, we use continuous-time Monte Carlo simulations (see Sec. IV) to study the dynamics of two interfaces in contact with each other in Sec. V and their steady-state properties in Sec. VI.

II. MODEL

In the BCSOS model of a single one-dimensional interface [1], the location or the height of the interface is described by a function $h(x,t)$ such that, for every lattice site $x=1,\ldots,L$ and $t\geq 0$,

$$h(x+1,t)-h(x,t)=\pm 1. \tag{1}$$

Due to these restrictions on local configurations, only two kinds of processes, adsorption and desorption, are available and the growth of the interface follows simple rules. In discrete time, if at some time step a randomly chosen lattice point x is a local minimum, then $h(x,t)$ increases (adsorption) by 2 with probability p, and if the chosen point is a local maximum, then it decreases (desorption) by 2 with probability q. For $p=q$ the BCSOS model describes an equilibrium system in the Edwards-Wilkinson (EW) universality class, and for $p\neq q$ it is known to be in the KPZ universality class [1,17]. In our continuous-time simulations (see Sec. IV), the parameters p and q correspond to respective transition rates per unit time.

We study the behavior of two coupled BCSOS interfaces h_1 and h_2. The coupling between them is produced by demanding that the interfaces cannot intersect:

$$h_1(x,t)\geq h_2(x,t) \quad \text{for all } x,t. \tag{2}$$

In all cases considered here, we impose the periodic boundary conditions $h_k(x,t)\equiv h_k(x+L,t)$ for $k=1,2$. We shall call the model of two BCSOS interfaces coupled in this way the BCSOS2 model.

In our model, there are four parameters (p_1,q_1,p_2,q_2) defining the transition rates for the interfaces h_1 and h_2, respec-

*janne.juntunen@phys.jyu.fi
†otto.pulkkinen@phys.jyu.fi
‡juha.merikoski@phys.jyu.fi

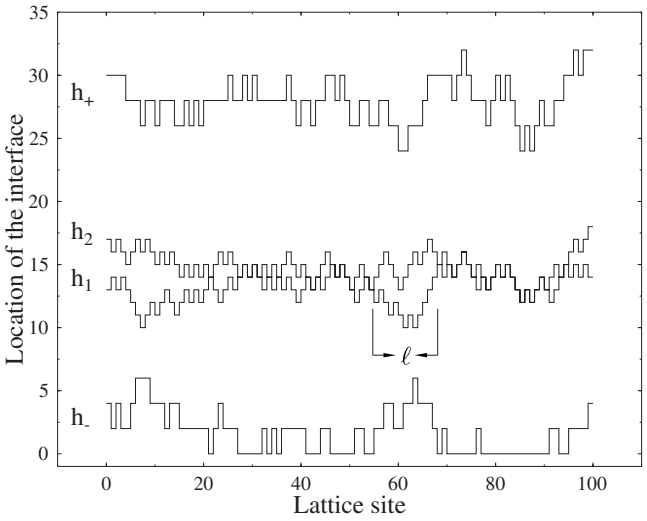

FIG. 1. Typical BCSOS interfaces h_1 and h_2 and the corresponding RSOS interfaces h_- and h_+. The symbol ℓ denotes the size of a "bubble" or "pore."

tively. To characterize the different regions of the parameter space, we found it convenient to use the following parameters:

$$r \equiv (p_2 - q_2)/(p_1 - q_1), \quad d_2 \equiv p_2/q_2. \tag{3}$$

It is of interest to consider also the sum and difference processes defined via

$$\left.\begin{aligned} h_+ &= h_1 + h_2 \\ h_- &= h_1 - h_2 \end{aligned}\right\} \Leftrightarrow \left\{\begin{aligned} h_1 &= \tfrac{1}{2}(h_+ + h_-), \\ h_2 &= \tfrac{1}{2}(h_+ - h_-). \end{aligned}\right. \tag{4}$$

The interfaces h_+ and h_- are of the restricted solid-on-solid (RSOS) type [1], obeying

$$h_\pm(x+1,t) - h_\pm(x,t) = -2, 0, +2. \tag{5}$$

The noncrossing condition of Eq. (2) is equivalent to

$$h_-(x,t) \geq 0. \tag{6}$$

An example of these interfaces is shown in Fig. 1.

Consider then the configuration-dependent adsorption and desorption rates

$$\tilde{p}_k(x,t) = p_k \delta(h_k(x,t) - h_k(x+1,t) + 1)\, \delta(h_k(x,t) - h_k(x-1,t) + 1),$$

$$\tilde{q}_k(x,t) = q_k \delta(h_k(x,t) - h_k(x+1,t) - 1)\, \delta(h_k(x,t) - h_k(x-1,t) - 1),$$

for $k=1,2$. When the interfaces h_1 and h_2 are locally away from each other, the corresponding rates for the evolution of the sum and difference process are $(\tilde{p}_+, \tilde{q}_+) = ((\tilde{p}_1 + \tilde{p}_2), (\tilde{q}_1 + \tilde{q}_2))$ and $(\tilde{p}_-, \tilde{q}_-) = ((\tilde{p}_1 + \tilde{q}_2), (\tilde{q}_1 + \tilde{p}_2))$. However, when the original interfaces are close to each other, then h_+ and h_- get coupled and the local transition rates are modified. If $h_-(x,t) = 0$ at time t in x and its neighboring lattice sites, then at x the corresponding rates for the sum and the difference processes become $(\tilde{p}_+, \tilde{q}_+, \tilde{p}_-, \tilde{q}_-) = (\tilde{p}_1, \tilde{q}_2, \tilde{p}_1 + \tilde{q}_2, 0)$. The dynamical rules for the interfaces h_+ and h_- produced by the BCSOS dynamics of h_1 and h_2 with the noncrossing condition are thus not those of the conventional RSOS model. Qualitatively, the process h_- resembles an RSOS interface in the presence of a solid wall, which has be used to model one-dimensional wetting in [18–20] and out of [21,22] equilibrium.

To characterize the statistical properties of the interfaces h_1 and h_2, and the sum and difference processes h_+ and h_-, we use their roughness or width [1] defined as

$$W_k(t) = \sqrt{\langle |h_k(x,t) - \bar{h}_k(t)|^2 \rangle}. \tag{7}$$

Here $k=1,2,+,-$ and $\bar{h}_k(t)$ is the spatially averaged height of the interface configuration at time t; the angular brackets denote ensemble average—i.e., an average over independent simulations.

III. OVERALL BEHAVIOR

At the mean-field level, the independent BCSOS interfaces are described by the continuum equation [17]

$$\partial_t h_k(x,t) \sim (p_k + q_k)\partial_x^2 h_k(x,t) + (p_k - q_k)\{[1 + \partial_x h_k(x,t)]^2\}, \tag{8}$$

where the first term on the right-hand side describes the interface tension $\nu_k \sim p_k + q_k$ and the second term including the nonlinear KPZ term is responsible for the propagation of the interface such that the velocity $\langle v_k \rangle_{\text{free}}$ of a free interface is proportional to the coefficient of the nonlinear term $\lambda_k \sim p_k - q_k$. The case $p_k = q_k$ results in scaling in the EW universality class [1]. In both the KPZ and EW cases, the stationary state of a free BCSOS interface is fully disordered [17]. We note that when the interfaces come in contact, this mean-field picture is not valid, but can nevertheless guide our understanding of some observations. In the stationary state of the BCSOS2 model, the final velocities of the interfaces, $\langle v_k \rangle_{\text{stat}}$, depend on their mutual interaction.

The parameter space of the BCSOS2 model can be divided into a few sections and its dynamics, depending on the initial state, into a few stages. We shall concentrate on the case where the two BCSOS interfaces h_1 and h_2 initially are apart from each other and propagate at such average velocities that they eventually meet and begin to interact—i.e., by choosing the parameters (p_1, q_1, p_2, q_2) such that $\langle v_2 \rangle_{\text{free}} > \langle v_1 \rangle_{\text{free}}$. Two particular realizations of interest are the *totally asymmetric case* $p_2 > p_1 > 0$ with $q_1 = q_2 = 0$, resulting in $\langle v_2 \rangle_{\text{free}} > \langle v_1 \rangle_{\text{free}} > 0$ and $\langle v_2 \rangle_{\text{stat}} = \langle v_1 \rangle_{\text{stat}} > 0$, and the *symmetric case* $p_2 = q_1 < p_1 = q_2$, resulting in $\langle v_2 \rangle_{\text{free}} = -\langle v_1 \rangle_{\text{free}} > 0$ and $\langle v_2 \rangle_{\text{stat}} = \langle v_1 \rangle_{\text{stat}} = 0$. In the symmetric case the interfaces are simply relaxing toward each other, after which their distance exhibits equilibrium fluctuations in the steady state. The asymmetric case retains its propagating, nonequilibrium characteristics also in the steady state.

The behavior of the interface roughness of the BCSOS2 model can be divided into a few stages. Consider first interfaces starting from a flat configuration. There are obviously three scenarios.

(A1) The interfaces first fully roughen independent of each other to their asymptotic roughnesses dependent on the system size, then start to interact, which initially will reduce their roughness by restricting the available configuration space, and finally reach together a steady state with individual roughnesses determined by their mutual interaction. The first stage proceeds according to the KPZ dynamics. Interface roughness can thus be a nonmonotonic function of time.

(A2) The interfaces meet each other essentially flat and then roughen together.

(A3) In the intermediate case the interfaces first have time to roughen independently only up to some length scales less than the system size L, then interact, and finally roughen again together to the stationary state.

Scenarios (A1)–(A3) can be realized by controlling the effective force F—e.g., the relative velocity $\langle v_2\rangle_{\text{free}}-\langle v_1\rangle_{\text{free}}$—driving the interfaces against each other such that in case (A1) F is the largest and in case (A2) it is the weakest.

In the case where the two interfaces both are initially rough—i.e., completely disordered—we find two scenarios.

(B1) For large F, the interaction of the two interfaces first reduces their roughness (or at least of one of them depending on the interaction parameters), after which they roughen together toward the stationary state. For very large F their dynamics is locked and their roughnesses become the same.

(B2) Also for small F, first a decrease in roughness is observed, but after that the roughness of an individual interface does not need to increase.

Another possibility, a reversed process—i.e., two interfaces escaping from each other and healing from mutual interaction—is not considered here.

Consider next the symmetric case and model the mutual repulsion between h_1 and h_2 by an exponential potential term in the equations of motion. The coupled KPZ equations for the symmetric case then read

$$\partial_t h_1 = \nu\partial_x^2 h_1 - \lambda(\partial_x h_1)^2 - \lambda + e^{\kappa(h_2-h_1)} + \eta_1,$$

$$\partial_t h_2 = \nu\partial_x^2 h_2 + \lambda(\partial_x h_2)^2 + \lambda - e^{\kappa(h_2-h_1)} + \eta_2,$$

where η_k denotes the noise and $\kappa>0$. For the sum process the potential terms cancel out,

$$\partial_t h_+ = \nu\partial_x^2 h_+ - \lambda(\partial_x h_+)(\partial_x h_-) + \eta_+, \tag{9}$$

but for the difference process, we obtain

$$\partial_t h_- = \nu\partial_x^2 h_- - 2\lambda - \frac{\lambda}{2}[(\partial_x h_+)^2 + (\partial_x h_-)^2] + 2e^{-\kappa h_-} + \eta_-. \tag{10}$$

Apart from the coupling term, this corresponds to the KPZ equation in the presence of a repulsive wall with a short-range potential [14,23]. Since the coefficients of the nonlinear term and the drift term are equal [see Eq. (8)], the wetting transition occurs at $\lambda=0$.

IV. NUMERICAL METHODS

In our Monte Carlo simulations, we used the continuous-time N-fold algorithm described by Bortz *et al.* [24]. In this algorithm, the possible transitions are divided into N classes according to their probabilities. After that one finds all lattice sites which belong to a certain class j. The next step is to calculate the time-dependent variables $Q_i=\Sigma_k^i n_{j_k} P_{j_k}$ for $i=1,\ldots,N$, where n_{j_k} is the number of those lattice points belonging to class j_k and P_{j_k} is the probability associated with that class. The class j of the event which will next occur is determined by finding j such that $Q_{j-1}\leq\xi<Q_j$, where ξ is a random number with a uniform distribution in the interval $[0,Q_N)$. After finding the class, one randomly chooses a location (which can be on h_1 or h_2 in our model) from this class and executes the transition. The time taken by this transition is then $\Delta t=-\ln(\xi)/Q_N$, where $\xi\in[0,1)$ is another random number from the uniform distribution.

In the numerical results shown for the BCSOS-type interfaces h_1 and h_2, we first computed separately the widths for even and odd lattice sites, $W_{k,\text{even}}$ and $W_{k,\text{odd}}$, respectively, and then calculated $W_k^2=W_{k,\text{even}}^2+W_{k,\text{odd}}^2$. This makes some phenomena more visible, because then a "flat" BCSOS configuration corresponds to $W_k=0$, while Eq. (7) used directly with all sites would give a finite roughness for it. For "rough" configurations this does not make a big difference. For the RSOS-type functions h_+ and h_-, the widths have been computed via simple variances over all sites. We use below the notation W_k^s for the stationary roughness of interface k.

All simulations were started from configurations drawn from the stationary distribution of two independent free BCSOS interfaces—i.e., from completely disordered states [17]. To obtain initial configurations obeying the noncrossing condition, the distance of the two interfaces was set to $\bar{h}_1(t=0)-\bar{h}_2(t=0)=L/2$. To sample the widths, we used 1000 independent Monte Carlo runs for the transient dynamics discussed in Sec. V, because in this case there was no particular need to smooth out the fluctuations. To obtain the stationary-state results shown in Sec. VI, we produced at least 10 000 independent configurations for each data point. Note that our choice of an apparently complicated rejection-free algorithm is essential for interfaces driven strongly against each other, because for those cases almost all moves would get rejected within standard Monte Carlo schemes.

V. SIMULATIONS OF TRANSIENT DYNAMICS

To demonstrate the generic behavior outlined above, we next show results of Monte Carlo simulations started from completely disordered BCSOS configurations of the two interfaces initially apart from each other.

We first consider the case $p_2>p_1>0$ and $q_1=q_2=0$. With this choice the dynamics of the interface h_1 is not affected by h_2 and the average velocities of the interfaces satisfy $\langle v_2\rangle\geq\langle v_1\rangle>0$, with $\langle v_2\rangle=\langle v_1\rangle$ only in the stationary state.

Starting from this case, where both interfaces propagate in the same (positive) direction and the second one eventually reaches the first one, we indeed see that the dynamics before the steady state can be divided into several stages. In Fig. 2, the effective force driving the interface h_2 against h_1, described here by the ratio $r=p_2/p_1$, decreases from top to bottom. First, the interfaces are independent of each other

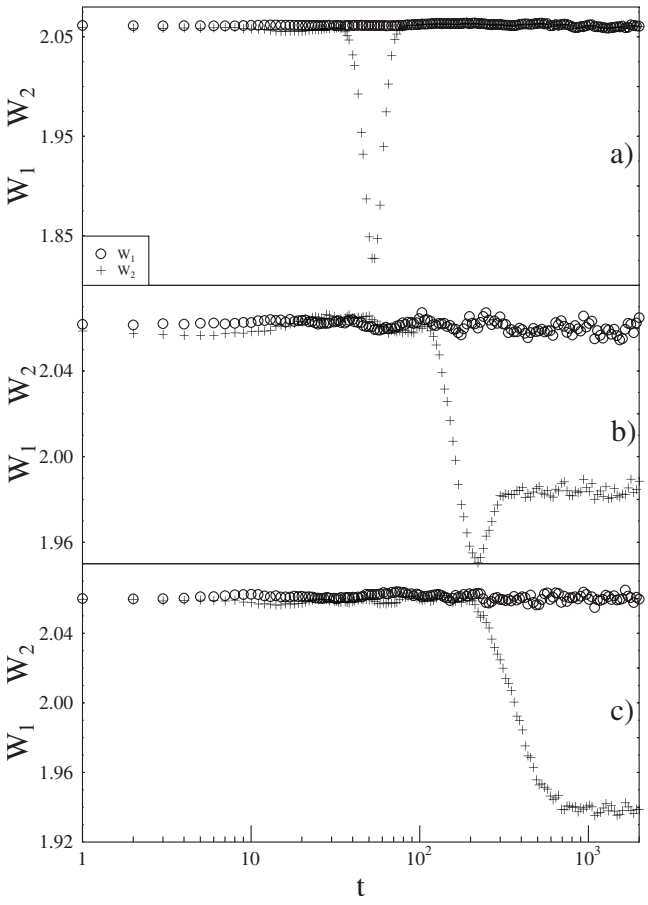

FIG. 2. Time dependence of the roughness of the processes h_1 and h_2 for a propagating pair of interfaces with (a) $p_1=0.1$, (b) $p_1=0.775$, and (c) $p_1=0.9$, in all cases with $p_2=1$, $q_1=q_2=0$, and $L=50$. At $t=0$ the interfaces h_1 and h_2 are completely disordered independent of each other with $\langle h_1\rangle-\langle h_2\rangle=L/2$.

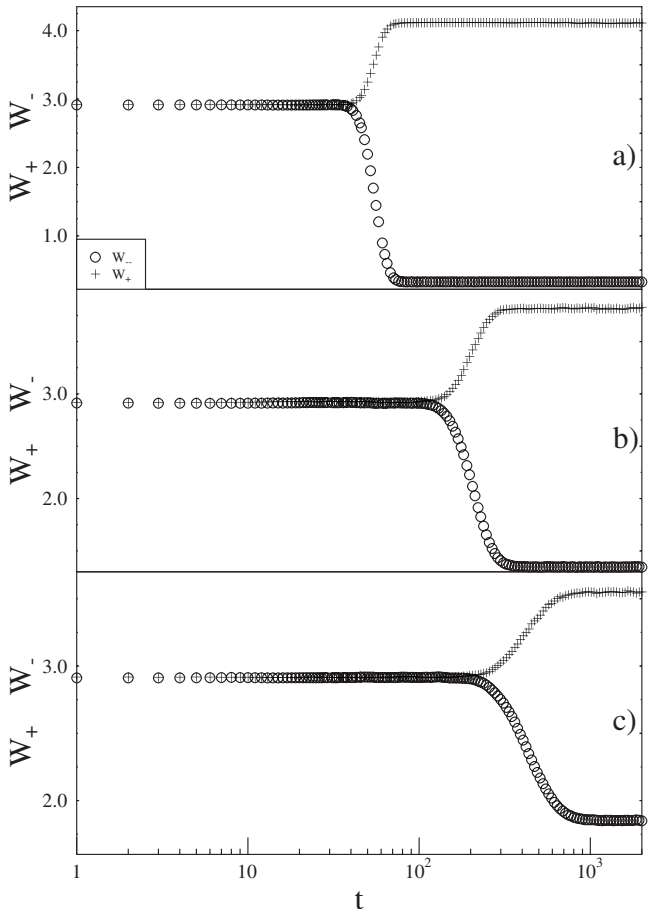

FIG. 3. Time dependence of the roughness of the sum and the difference processes h_+ and h_-, respectively, from the same simulations of the propagating pair of interfaces as in Fig. 3.

and evolve as free BCSOS interfaces. With these initial conditions both interfaces are fully disordered until they meet. In the second stage the interaction starts, which first reduces the roughness W_2 by restricting the configuration space available for the interface h_2. After that it can increase again when the shape of the interface h_2 conforms with that of h_1, almost completely for strong driving—i.e., for large r as in Fig. 2(a).

The time evolution of the roughness of the corresponding sum and difference processes h_+ and h_- is shown in Fig. 3. As expected, the roughness of the sum process, W_+, can only increase, because in time the shape of the interface h_2 more and more closely follows that of h_1. For the same reason, the process h_- decreases on average and therefore W_- decreases.

In Fig. 4, we show the behavior of the roughness of interfaces driven symmetrically toward each other: $p_1=q_2$ and $p_2=q_1$. The parameters have been chosen to correspond to those of the asymmetric process of Figs. 2 and 3 from the point of view of the effective force driving the interfaces against each other. Now the interfaces equally influence each other, while in the first case their interaction was in one direction only. The roughness of both interfaces first decreases. In the symmetric case, the time scale required for reaching the stationary state appears to be longer than in the propagating case. Again, the widths $W_\pm$ are monotonic in time (data not shown).

VI. SIMULATIONS OF THE STATIONARY STATE

We shall now inspect the dependence of the roughness on the system size and other parameters in the stationary state.

A. Propagating pair of interfaces

Again, we first consider the case $p_2>p_1>0$ and $q_1=q_2=0$. This section of parameter space contains also the cases for which transient dynamics was shown in Figs. 2 and 3.

As expected and seen in Fig. 5, in the case where the two BCSOS interfaces are asymptotically independent ($r=1$), the stationary widths scale as a function of the system size like $W^s_{1,2,-}\sim L^\alpha$ with $\alpha=1/2$. The behavior of the sum process (not shown) is, of course, similar. For $r<1$, when the interfaces are not independent, the size dependence of the roughness of the difference process, W^s_-, follows the same power law for small L, up to some scale determined by the effective force driving the interfaces toward each other, after which it saturates to a finite value.

From Fig. 6 one can observe that the stationary width W^s_1 of the interface h_1 is independent of the value of the driving

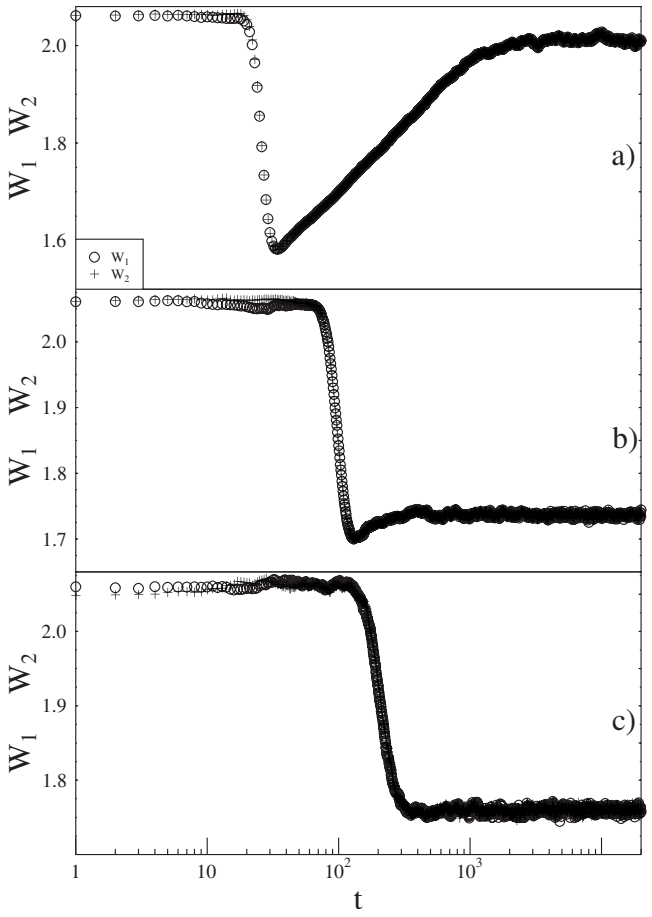

FIG. 4. Time dependence of the roughness of two interfaces h_1 and h_2 relaxing toward each other with the transition rates related to those in Figs. 2 and 3 such that the value of $d_2 \equiv 1/d_1$ in this case is same as r in the previous one with (a) $r=1/0.1$, (b) $r=1/0.775$, and (c) $r=1/0.9$, in all cases for $L=50$.

parameter r, as it should since the interface h_2 does not constrain the behavior of the interface h_1. However, the stationary width W_2^s is nonmonotonic as a function of the parameter r: First, as the interaction of the interfaces is increased, W_2^s decreases, because the interface h_1 constrains the interface h_2. For $r \to \infty$ the interfaces become strongly coupled and therefore it follows that $W_2^s \to W_1^s$.

Since h_2 does not behave like a free BCSOS interface, also the properties of h_- are changed. In Fig. 7 we look at the behavior of W_-^s as a function of $r-1$. For large r, it becomes independent of L. For small r, there is a crossover to a different behavior and, finally, for $r \to 0$ we see W_- converging to a size-dependent value which is twice the stationary roughness of an isolated completely disordered BCSOS interface due to the cancellation of the cross-terms from $\langle [h_1 - h_2 - (\bar{h}_1 - \bar{h}_2)]^2 \rangle$ in this limit.

The behavior of W_-^s as a function of r for $r \gg 1$, as seen in the inset, is easy to explain. In this limit, the "excitations" in $h_- = h_1 - h_2$ become small isolated pores (see Fig. 1), each of which gives independent "counts" in the sampling of $(W_-^s)^2$. The probability for the existence of the smallest possible pore is proportional to r. Therefore one expects $W_-^s \sim \sqrt{r}$, as seen in the simulation data.

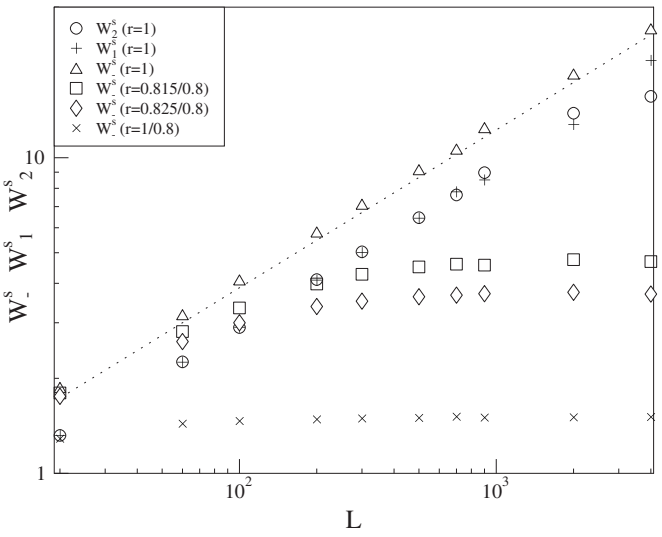

FIG. 5. The size dependence of the stationary widths for a propagating pair of interfaces h_1 and h_2 and their difference h_- interfaces for a few values of the parameter r. The slope of the dotted line corresponds to the value of the roughness exponent $\beta = 1/2$.

B. Interfaces driven symmetrically toward each other

In the symmetric case $p_1 = q_2$ and $p_2 = q_1$, we describe the strength of the interaction between the interfaces by the parameter $d_2 = p_2/q_2$. In this case, $W_1^s = W_2^s$. As seen in Fig. 8, they both qualitatively behave like W_2^s for the propagating case in Fig. 6. The stationary roughness is a nonmonotonic function of the driving parameter d_2, and there is a pronounced minimum in it. Also, $W_1^s(d_2 \leq 1) = W_1^s(d_2 \to \infty)$. For increasing L the location of the minimum moves to the left—i.e., toward $d_2 = 1$—which corresponds to the case of noninteracting interfaces. In the inset we show our best data collapse for the dip bottom with a finite-size scaling described by the scaling exponent value 1/3. In the scaling limit $L \to \infty$, the roughness becomes discontinuous at $d_2 = 1$.

The dip prevails for large system sizes due to correlations generated by the interaction between the interfaces. One

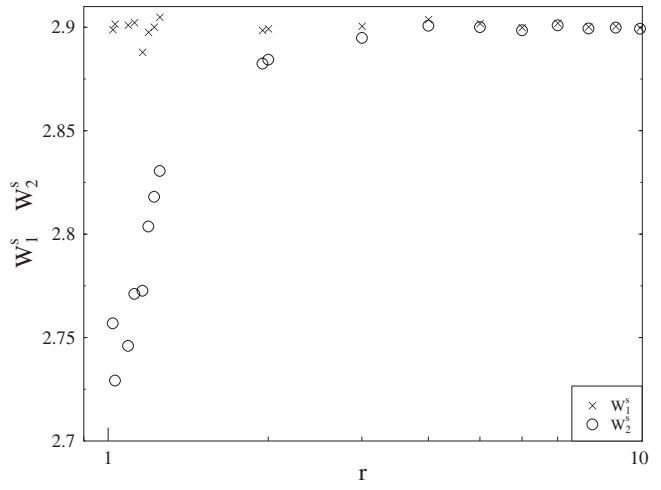

FIG. 6. The stationary widths $W_{1,2}^s$ as a function of the parameter r for a propagating pair of interfaces with $L=100$.

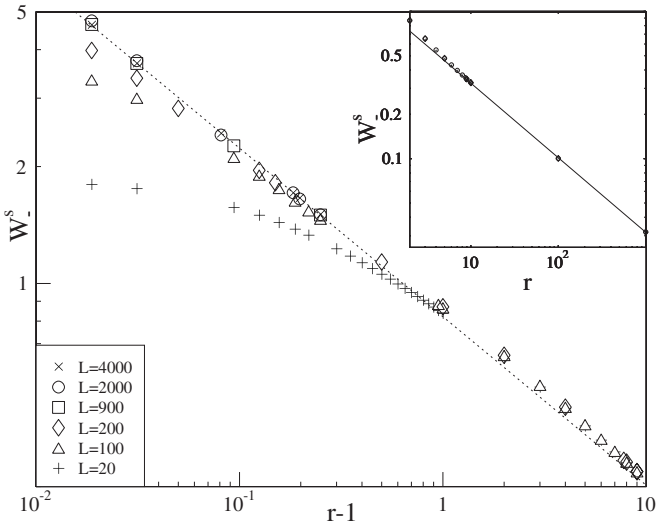

FIG. 7. The stationary width W^s_- as a function of $r-1$. The slope of the dotted line is -0.434. The inset shows the same data as a function of r. The slope of the fitted line is -0.506.

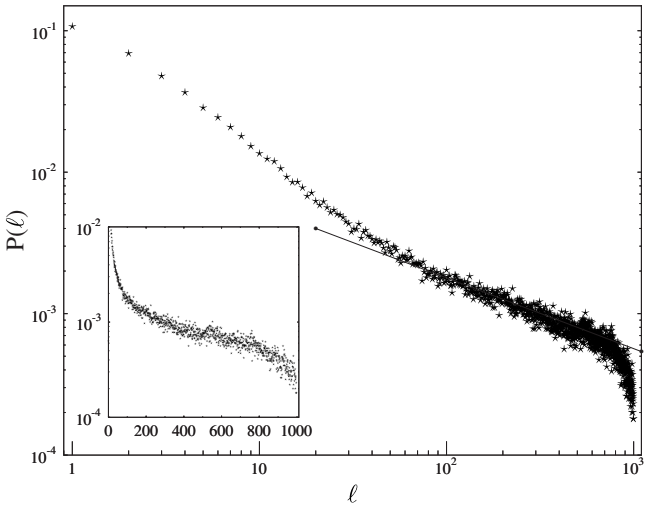

FIG. 9. The stationary pore size distribution for the relaxing case with symmetric dynamics $p_1=q_2=0.4998$ and $q_1=p_2=0.5002$ and $L=1000$. The slope of the fit in the power-law regime is -0.5.

measure of these correlations is the pore size distribution, which contains more information than the scaling of the interface width alone [1,25,26]. An example of a pore-size distribution for a small value of d_2 (leading to large bubbles) is shown in Fig. 9. A power law is observed before the exponential cutoff by finite-size effects at large pore sizes. The value of the exponent, 1/2, is consistent with the return time exponent for a single random walker run against a smooth fixed wall [27].

To obtain the numerical results discussed above, we used continuous-time Monte Carlo simulations in discrete space with discrete height increments. In addition, we checked that the results for the dip region do not considerably change with

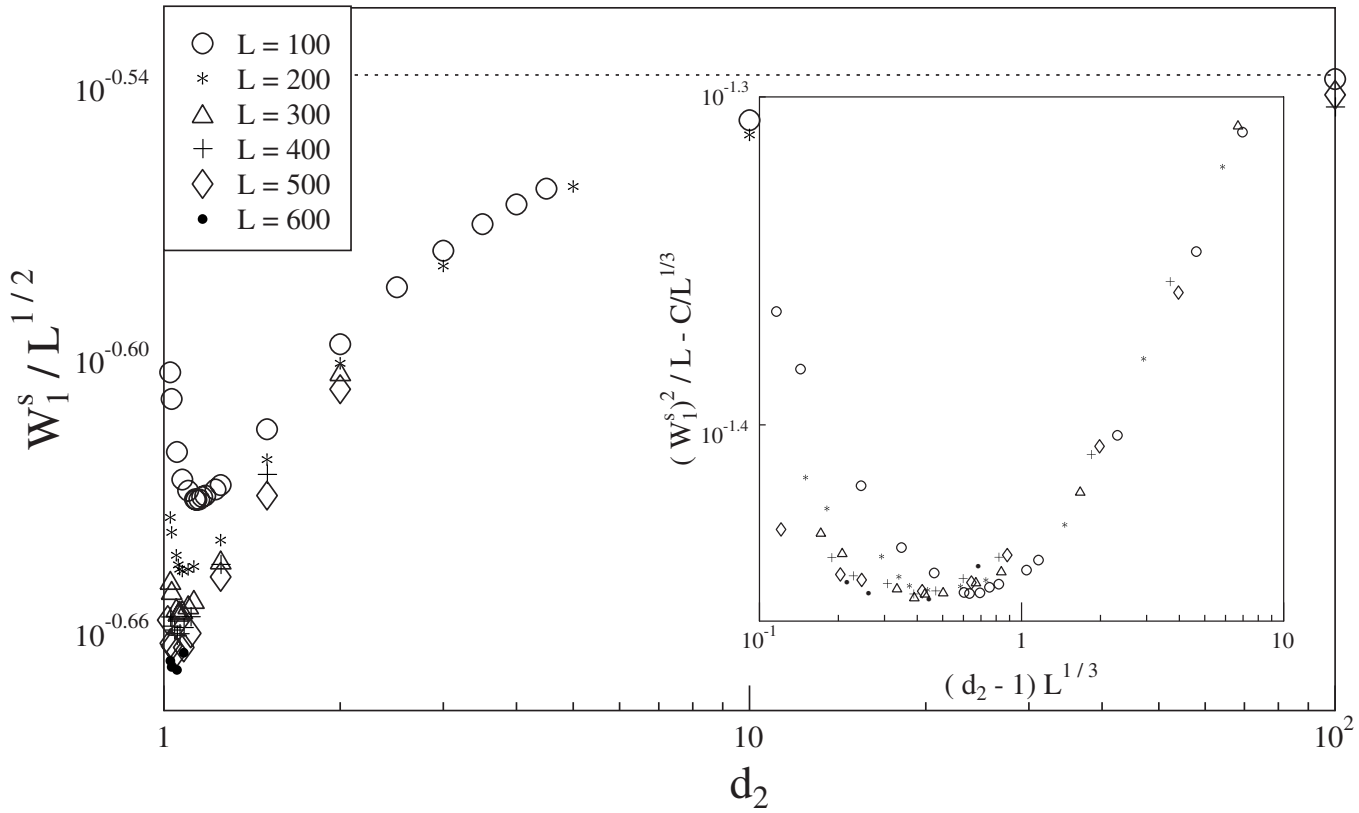

FIG. 8. The stationary width W^s_1 scaled by $L^{-1/2}$ for interfaces driven symmetrically against each other—i.e., an example of the equilibrium case—as a function of the parameter d_2. The dashed line indicates the stationary width of an isolated interface. The inset shows the scaling plot for the dip bottom.

standard discrete-time Monte Carlo dynamics. To further check the possible effects of discreteness of the height variable, we also performed direct numerical integration of two coupled KPZ equations with a continuous height variable and observed the nonmonotonic behavior of the width for this case also.

VII. CONCLUSIONS

To summarize, we have proposed a model consisting of two interacting nonintersecting BCSOS interfaces and studied the behavior of the interface roughness in it. Different scaling scenarios depending on the initial conditions and the values of the parameters were identified and numerically analyzed. We decomposed the combined process into sum and difference processes, the widths of which evolve in time and as functions of the interaction strength at different rates. This results in a nonmonotonic behavior of the roughness of the original interfaces, which prevails up to large system sizes and is related to correlations carried by the pores between the points of contact of the interfaces.

ACKNOWLEDGMENTS

We acknowledge useful discussions on random walks with Perttu Luukko. This work was supported by the Academy of Finland.

[1] A.-L. Barabasi and E. H. Stanley, *Fractal Concepts in Surface Growth* (Cambridge University Press, Cambridge, England, 1995).
[2] P. Meakin, *Fractals, Scaling and Growth far from Equilibrium* (Cambridge University Press, Cambridge, England, 1998).
[3] A.-L. Barabasi, Phys. Rev. A **46**, R2977 (1992).
[4] R. A. da Silveira and M. Kardar, Phys. Rev. E **68**, 046108 (2003).
[5] S. N. Majumdar and D. Das, Phys. Rev. E **71**, 036129 (2005).
[6] A. J. Bray, Adv. Phys. **43**, 357 (1994).
[7] M. Kardar, Physica A **263**, 345 (1999).
[8] B. Drossel and M. Kardar, Phys. Rev. Lett. **85**, 614 (2000).
[9] J. Zhang, Y.-C. Zhang, P. Alstrom, and M. T. Levinsen, Physica A **189**, 383 (1992).
[10] M. Myllys, J. Maunuksela, M. J. Alava, T. Ala-Nissila, J. Merikoski, and J. Timonen, Phys. Rev. E **64**, 036101 (2001).
[11] A. S. Balankin, R. G. Paredes, O. Susarrey, D. Morales, and F. C. Vacio, Phys. Rev. Lett. **96**, 056101 (2006).
[12] P. Ferrari and M. Praehofer, Markov Process. Related Fields **12**, 203 (2006).
[13] O. A. Hammal, F. de los Santos, and M. A. Munoz, J. Stat. Mech.: Theory Exp. (2005) P10013.
[14] M. A. Munoz, in *Advances in Condensed Matter and Statistical Physics*, edited by E. Korutcheva, G. Nadjakov, and R. Cuerno (Nova Science, Hauppauge, NY, 2004).
[15] M. A. Munoz, F. de los Santos, and A. Achahbar, Braz. J. Phys. **33**, 443 (2003).
[16] H. L. Richards and T. L. Einstein, Phys. Rev. E **72**, 016124 (2005).
[17] J. Neergaard and M. den Nijs, J. Phys. A **30**, 1935 (1997).
[18] V. Privman and N. M. Svrakic, Phys. Rev. B **37**, 3713 (1988).
[19] V. Privman and N. M. Svrakic, J. Stat. Phys. **51**, 1111 (1988).
[20] V. Privman and M. C. Bartelt, Z. Phys. B **78**, 501 (1990).
[21] H. Hinrichsen, R. Livi, D. Mukamel, and A. Politi, Phys. Rev. E **68**, 041606 (2003).
[22] F. de los Santos, M. M. Telo da Gama, and M. A. Munoz, Phys. Rev. E **67**, 021607 (2003).
[23] O. Al Hammal, F. de los Santos, M. A. Munoz, and M. M. Telo da Gama, Phys. Rev. E **74**, 011121 (2006).
[24] A. B. Bortz, M. H. Kalos, and J. L. Lebowitz, J. Comput. Phys. **17**, 10 (1975).
[25] J. J. Ramasco, J. M. Lopez, and M. A. Rodriguez, Phys. Rev. Lett. **84**, 2199 (2000).
[26] M. Kardar, G. Parisi, and Y. C. Zhang, Phys. Rev. Lett. **56**, 889 (1986).
[27] W. Feller, *An Introduction to Probability Theory and its Applications* (Wiley, New York, 1968), Vol. 1.